The International Journal of Advanced Manufacturing Technology
https://doi.org/10.1007/s00170-020-05725-9

ORIGINAL ARTICLE

The joining of gamma titanium aluminides via the powder interlayer bonding method

P. D. Davies[1] · H. M. Davies[1] · I. Watkins[1] · D. A. Britton[1]

Received: 6 February 2020 / Accepted: 6 July 2020

Abstract
Powder interlayer bonding (PIB) is a joining technique originally developed to enable high-integrity repairs of aerospace components. The technique has previously been employed for the joining of titanium and nickel alloys utilised in the aerospace industry. This study expands on the application of the novel joining technique known as powder interlayer bonding (PIB), to the bonding of γ titanium aluminide (TiAl) material. PIB has been used to facilitate high-integrity joints in gamma titanium aluminides (TiAl), where full densification of the joint was achieved. The PIB technique described here used a metallic powder interlayer between the two faying surfaces of γ TiAl specimens. Bonds were formed in an inert atmosphere under induction heating. The PIB technique proved capable of producing high-integrity bonds in terms of microstructural evaluation, with very limited porosity retained after the bonding cycle. A brittle Ti_2Al phase can be produced with heavily oxidised powder which is susceptible to cracking and will negatively affect mechanical properties.

Keywords Powder interlayer bonding (PIB) · Gamma titanium aluminides

1 Introduction

Gamma titanium aluminides have been under consideration for over 30 years for use in the aerospace and automotive sectors [1–4], with research concentrated mainly on titanium aluminide (TiAl) alloys that contain minor fractions of the α_2 (Ti_3Al) phase. Applications considered include turbine components such as compressor stator vanes, LP turbine blades [5] and automotive valves [3]. Indeed, such alloys are already in use as blades within GEnxTM engines and the new β-stabilised TiAl alloy (TNM) is being used to manufacture LPT blades for PW1100G™ engines [1, 4].

Being intermetallic in nature, with inherent brittleness, intricate composition and microstructure, γ-TiAl alloy metallurgy can be very challenging. Figure 1 illustrates the phase diagram proposed by Schuster and Palm after their reassessment of the binary aluminium-titanium phase diagram [6]. Major advances have been made in the development of the TiAl alloy system, with Al contents between 44 and 48 at.%. According to Schuster and Palm [6], these engineering alloys solidify via the β phase or a peritectic reaction. An eutectoid transformation $\alpha \rightarrow \alpha_2 + \gamma$ occurs on cooling in all engineering γ (TiAl) alloys. To preserve thermodynamic equilibrium in alloys whose compositions stray from the eutectoid composition, the volume fraction of the γ (TiAl) phase increases rapidly as the eutectoid transformation temperature is crossed.

As with many engineering alloys, composition and processing route play a vital role in determining the resultant microstructure and associated mechanical properties [4], with a wide variety of microstructures ranging from duplex to fully lamellar structures being possible [7]. Fine microstructures generated either by high-temperature processing or by rapid cooling contain a high proportion of α_2. These structures are considered to provide the best balance of properties, since room temperature properties are generally enhanced but with no significant reduction in creep properties. The cooling rates employed to develop fine microstructures are often too aggressive to result in thermodynamic equilibrium, and therefore the microstructures obtained may not be stable. During exposure to typical operating temperatures, these fine structures can demonstrate a relatively rapid loss of properties [4].

Further alloying additions have been shown to produce a range of microstructures with beneficial mechanical properties [4]. The effect of aluminium on the mechanical properties has

✉ P. D. Davies
p.d.davies@swansea.ac.uk

[1] Institute of Structural Materials, College of Engineering, Swansea University, Bay Campus, Fabian Way, Swansea SA1 8EN, UK

Published online: 25 July 2020

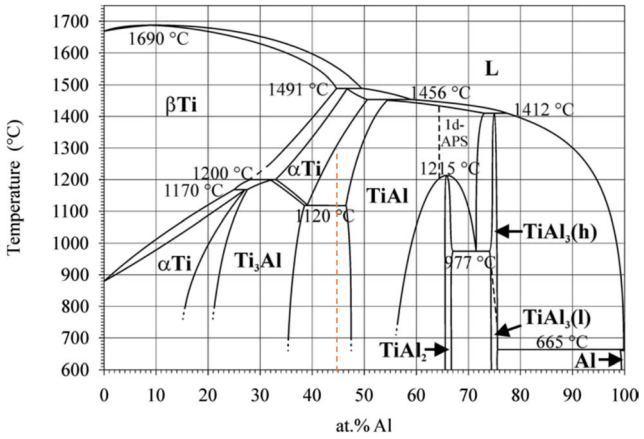

Fig. 1 Binary TiAl phase diagram [6] with composition of Ti–45Al–2Nb–2Mn + 0.8 vol.% TiB_2 alloy identified by dotted red line

been complicated by more recent developments in processing, where hot extrusion methods deliver ductility levels unattainable via a traditional casting route. The effect of aluminium on strength is more defined where lower aluminium contents have been shown to improve the strength of binary alloys [8], which is believed to be a result of an increased α_2 content. In contrast, higher aluminium contents are preferred where a resistance to oxidation is required. Niobium and other refractory elements provide improvements in strength, creep resistance and oxidation resistance, while additions of up to 2% manganese have been shown to improve ductility [9]. Boron is utilised as grain a refiner at contents of up to 1% through the XD process where refined lamellar colonies in cast microstructures can be developed [10]. Ti-45-2-2-XD has been used to make several different aeroengine components by Rolls-Royce Plc; compressor stator vanes and blades, low pressure turbine blades and large complex cast components.

For TiAl alloys to be widely incorporated in future aeroengine builds, they will be required to be joined to themselves and other alloys and offer the option of being repaired. Several joining techniques widely used in the aeroindustry such as tungsten inert gas (TIG) welding [11], electron beam welding (EBW) [12–15] and laser beam welding (LBW) [16] have been used to join TiAl alloys with varying success. Due to a combination of their inherent low ductility and the high thermal stresses produced during joining, solid-state cracking can be a major concern when joining TiAl alloys using fusion joining techniques, though this effect can be alleviated by careful manipulation of welding parameters, where preheating to 700–800 °C is recommended to avoid solidification cracking. During their work on the Ti–45Al–2Nb–2Mn + 0.8 vol.% TiB_2 alloy, Chaturvedi et al. [12] recommend that the α-γ phase transformation not be suppressed during EBW, suggesting that the critical cooling rate at the fusion zone boundary is 250 K s^{-1}. Solid-state joining techniques such as diffusion bonding (DB), have been utilised where TiAl alloys have been bonded to themselves [17, 18]; other alloys [19], and utilising interlayers [20, 21] without the concern of solid-state cracking. However, the formation of the brittle α_2 phase along the bond line during DB can degrade mechanical properties due to the development of favourable crack paths [18]. Diffusion brazing [22], diffusion welding [23] and induction brazing [24, 25] have all been used to join TiAl alloys without solid-state cracking. Friction welding of TiAl alloys to steel using copper interlayers [26] has been performed but again solid-state cracking proved to be of concern. While many techniques have been used to join TiAl alloys on a laboratory scale, actual aeroengine components are notoriously difficult to join and repair via conventional fabrication routes. The availability of high-integrity joining techniques for these components will offer opportunities for future design configurations and reduce component life cycle costs via repair. Powder interlayer bonding (PIB) has already proved it can be used to provide high-integrity bonds between aerospace alloys [27]. PIB is a novel joining technique capable of producing high-integrity bonds that may provide opportunities to save otherwise redundant aeroengine components [28]. The PIB technique uses a metallic powder interlayer between the two bonding surfaces being joined; this reduces surface asperities and the dependency of the joining process on smooth surface finishes. An inert gas is used to shield the fusion zone from oxidation during joining process, with heat supplied by induction heating. PIB offers

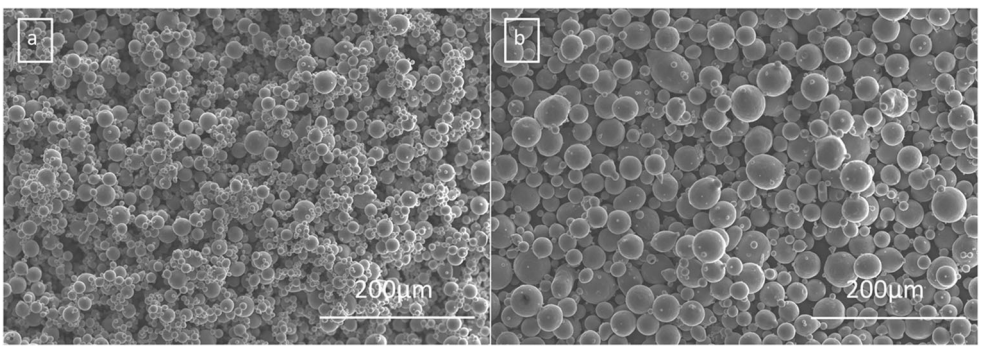

Fig. 2 Ti–45Al–2Nb–2Mn + 0.8 vol.% TiB_2 XD as received powders used in this study, **a** sub 25 µm and **b** 25–45 µm

Table 1 Bonding parameters used during this study

Bond	Temp (°C)	Time (min)	Pressure (MPa)	Powder diameter (μm)
1	1080	60	32	25–45
2	1120	60	32	25–45
3	1120	60	32	< 25

advantages over many of the previously mentioned joining techniques such as low cost, localised heating, narrow fusion zone, reduced residual stress in the bond region and future portability, which will be a major advantage for repairing gas turbine components.

2 Experimental

Material was supplied in the form of a cast ingot, with a specified composition of Ti–45Al–2Nb–2Mn + 0.8 vol.% TiB_2 prepared by the XD process and hot-isostatic-pressed at 1250 °C (± 10 °C) for 4 hours (+ 15 min/− 0 min) at a pressure of 140 MPa (± 5 MPa) under an argon atmosphere. After HIPping, the castings were vacuum heat–treated at 1010 °C (± 10 °C) for 8 h (+ 15 min/− 0 min), followed by furnace cooling to below 500 °C. An argon gas quench was then used to cool to below 150 °C.

The spherical Ti–45Al–2Nb–2Mn + 0.8 vol.% TiB_2 powders used in this study which were supplied by TLS Tecknik GmbH & Co are illustrated in Fig. 2a, b, with powder particles either having diameters between 25 and 45 μm or sub 25 μm. Powder interlayers were created by combining Ti–45Al–2Nb–2Mn + 0.8 vol.% TiB_2 powder with cellulose powder, glycerol and deionised water to create a paste. The paste was then applied to the surface of one of the specimens. Prior to applying paste and attaching thermocouples, bonding specimens were ultrasonically cleaned in industrial acetone for 30 min.

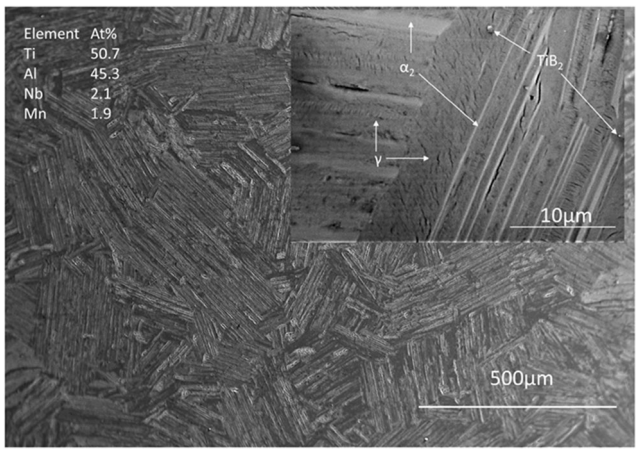

Fig. 3 Microstructure of Ti–45Al–2Nb–2Mn + 0.8 vol.% TiB2XD as received material, including analysed composition

Bonding was performed in an argon environment where parts were shielded from the local environment. Bonding was performed as per the conditions listed in Table 1. The bond regions of both alloys were initially heated by a water-cooled induction coil to 1000 °C, at a heating rate of approximately 6 °C s. In order not to exceed the bonding temperature, a second heating rate of 0.5 °C s was then employed to achieve the final temperatures in either the $\alpha + \gamma$ or $\alpha_2 + \gamma$ regions. Specimens were held at temperatures (± 5 °C) for 60 min. When joining was completed, the bonded specimens were air-cooled to room temperature. Temperature was measured by type N thermocouples welded in place within 1 mm of the faying surface and connected to a calibrated Fluke 54 II thermometer.

To facilitate metallographic analysis, the specimens were mounted in conductive Bakelite. Specimens were then prepared via a standard grinding and polishing procedure concluding with a final polish using a non-crystallising colloidal silica solution (0.04 μm). The samples were etched with Krolls Reagent for approximately 5 s. The microstructural characterisation was performed using a Hitachi SU3500 scanning electron microscope (SEM) equipped with energy-dispersive spectroscopy (EDS) facilities. Hardness measurements were performed on a Struers Duramin 40 hardness tester. All testing was performed with a force of 1 kg and dwell time of 10 s, in accordance with ASTM standards. Measurements were taken at the bond line and at locations 25 μm, 50 μm, 1 mm, 2 mm, and 3 mm away.

3 Results

The processing route results in a fully lamellar structure of thin α_2 laths in a matrix of thicker ɣ laths. These are arranged in 'packets', which are regular in shape, as illustrated in Fig. 3. The addition of titanium diboride in this alloy causes small precipitates to form due to an exothermic-dispersion composite fabrication process [29]. The average packet size was found to be ~ 240 μm, with minimum and maximum values of 150 μm of 300 μm respectively. The α_2 laths are identifiable as light-coloured needle-like structures (average thickness of ~ 1.4 μm). In some packets, they appear to be of a similar width to the darker ɣ phase (average thickness of ~ 4.6 μm), but generally they were found to be much thinner.

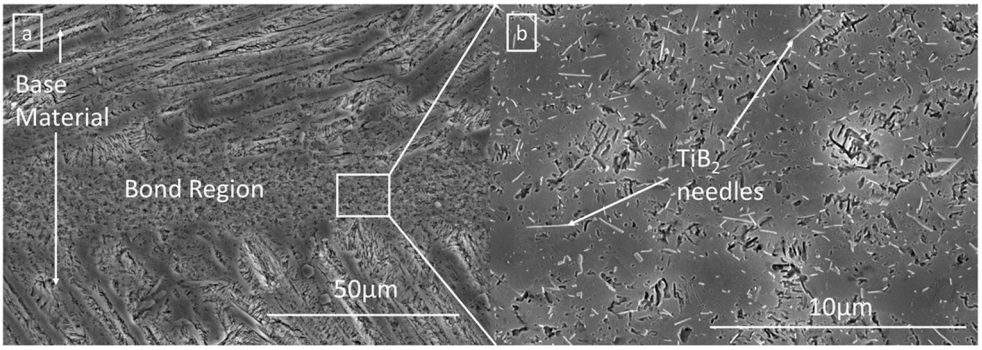

Fig. 4 **a** Comparison of the microstructure of bond 1 through the base material and bond region, **b** TiB_2 needles seen throughout bond line

The microstructure of the bond region from bond 1 is illustrated Fig. 4a. The bond line was found to be ~ 20 μm thick through the centre region of the bond. Complete densification of the bond was achieved in some regions. Many needle-like TiB_2 precipitates can be seen throughout the bond region as illustrated in Fig. 4b, the somewhat porous-looking structure is due to precipitate pull-out during the grinding and polishing procedure. However, there were instances of retained porosity found surrounding powders that had not fully collapsed during the bonding cycle, with a maximum pore size of ~ 7 μm as illustrated in Fig. 5a. The bond region of bond 2 was found to be very similar in appearance to bond 1; however, full collapse of the powder interlayer had occurred. There were very limited instances of retained porosity seen throughout bond region with a maximum pore size of ~ 2 μm, as illustrated in Fig. 5b. The bond region of bond 3 formed with sub 25 μm powder again shows similarities with those of bonds 1 and 2, with almost complete densification, very limited retained porosity, with maximum pore sizes being sub-micron, as shown in Fig. 6a. However, numerous instances of a brittle Ti_2Al phase, up to 60 μm in length, were found throughout the bond region. A number of these were found to have cracked on cooling from the bonding temperature as illustrated in Fig. 6b.

Hardness results for the 3 bonds are illustrated in Fig. 7. Peak hardness values are similar for all 3 bonds, ranging from HV433 for bond 1 to HV452 for bond 3. Peak values appear at the bond line, before declining quickly and returning to baseline levels.

4 Discussion

It has already been shown that PIB can be used to provide high-integrity bonds between aerospace alloys [27, 30–32]; so, it is no surprise to see high-integrity bonds being produced in the TiAl alloy. The joint is formed through a solid-state sintering process, where the combination of thermal energy and applied load act to consolidate and densify the powder. Bonding is facilitated by a reduction in the total interfacial energy resulting from the densification and changes to the interfacial area. As described in previous work [27], the bonding process can be viewed as three associated phases: the initial, intermediate and final phases. Localised bonding occurs between adjacent powders through the formation of necks during the initial phase, resulting in a small amount of plastic deformation as illustrated in the Ti-6Al-4 V alloy [32]. Continued growth of the necks requires material to be transported to this region via diffusion mechanisms such as volume and surface diffusion, where vacancies move from the neck region through the powder or along the surface of the powder respectively[33]. As bonding through the intermediate phase progresses, continued plastic deformation densifies the powder interlayer before slowing as the total surface area of the powders reduces until finally ceasing as previously illustrated [32]. Final densification and pore elimination occurs during the final phase where recrystallisation is facilitated by the stored energy introduced during the earlier deformation.

In order to limit deformation during the bonding cycle, the temperature of 1080 °C for bond 1 was chosen to produce the

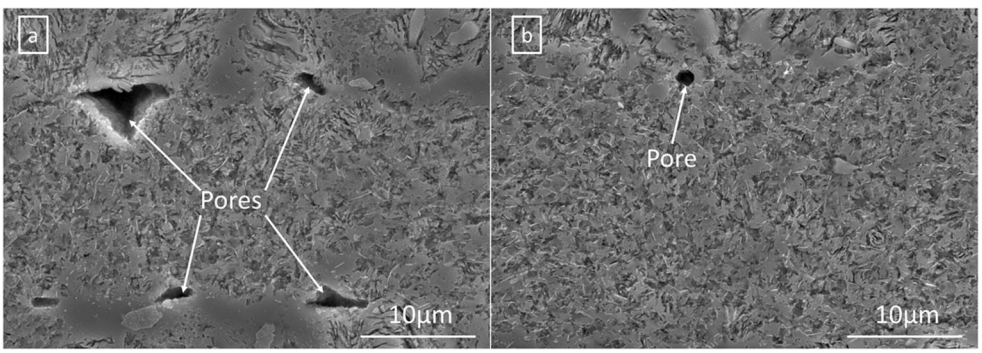

Fig. 5 Retained porosity found in **a** bond 1, **b** bond 2

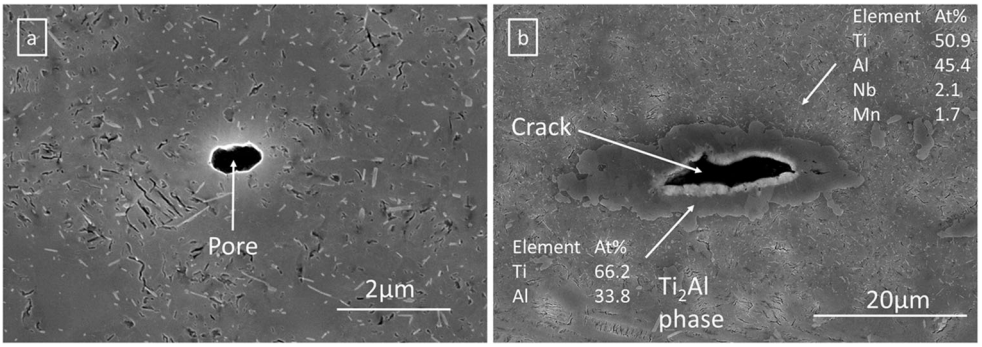

Fig. 6 **a** Retained porosity found in bond 3, **b** cracking discovered in Ti_2Al phase found in bond 3

bond in the $\alpha_2 + \gamma$ region. However, the combination of temperature, pressure and time failed to fully collapse the powder particles throughout the bond line. The combination of these processing parameters has been shown to be critical to achieving powder consolidation [27] as plastic deformation during the intermediate phase of the bonding cycle can be a major factor in the densification of the powders. If only partial powder collapse is achieved, then excessive pore size results which cannot be eliminated during the final phase. As seen in Fig. 5a, this resulted in several locations were retained porosity was discovered around the original circumference of individual powders. Although maximum pore sizes were relatively small, it was believed that these could be reduced further if full collapse of powder particles could be achieved. As a result of the exponential relationship between temperature and atomic diffusion, increases in temperature strengthen the impetus for densification and greatly affect process kinetics. Hence, bond 2 was produced at the higher temperature of 1120 °C, putting it in the $\alpha + \gamma$ region of the phase diagram. Previous PIB work [32] has highlighted that increasing the bonding temperature can refine porosity through the powder interlayer. As illustrated in Fig. 5b, the increase in temperature while holding time and pressure constant, facilitated full powder collapse throughout the powder interlayer. The ensuing diffusion of material was then able to reduce the maximum pore size significantly from ~ 7 to ~ 2 µm. Previous unpublished work on PIB has illustrated another way to reduce retained porosity density and size is to refine the powder particle diameter. This allows for tighter initial packing of the powder particles and smaller initial pore size following powder collapse. The subsequent diffusion of material is then able to close off the remaining pores to a greater degree resulting in a sub-micron maximum pore size as illustrated in Fig. 6a. However, as illustrated in Fig. 6b, there were frequent instances of a brittle Ti_2Al phase throughout the bond region. Although the sub 25 µm and 25–45 µm powder had been produced at the same time and from the same feed stock, the sub 25 µm had been previously used and hence exposed to the atmosphere. This resulted in the powder oxidising over the following months, promoting the formation of the Ti_2Al phase throughout the bond region. There have been no instances of this brittle phase when relatively fresh powder has been used. Figure 7 shows a clear trend in hardness for all 3 bonds, increasing on average ~ 60% in the bond line when compared with the baseline values for the bulk material. This trend has been found in previous work on PIB and can be explained by the finer grain structure throughout the bond region.

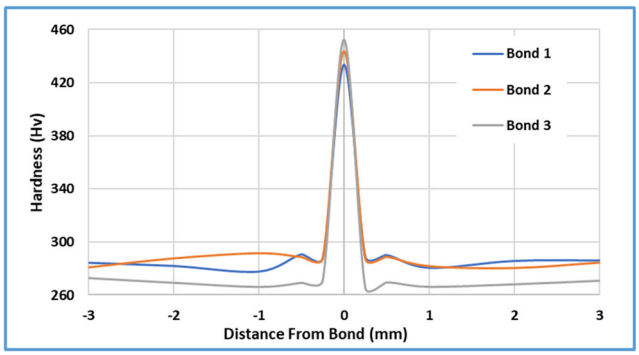

Fig. 7 Hardness results for bonds 1–3

5 Conclusions

- Powder interlayer bonding has proved to be a suitable process for producing high-integrity bonds in the TiAl alloy.
- Bonding at 1120 °C, in the $\alpha + \gamma$ region of the phase diagram, produced a fully consolidated bond in the TiAl alloy.
- Bonding at 1120 °C reduced the maximum pore size when compared `with the bonding at 1080 °C when time and pressure are kept constant.
- Refining the powder particle size is an effective method of reducing maximum pore size with the PIB process.
- Powder quality and condition is extremely important for producing high-integrity bond via the PIB process, where excessively oxidised powder can have a negative effect on bond quality.

References

1. Bewlay BP, Nag S, Suzuki A, Weimer MJ (2016) TiAl alloys in commercial aircraft engines. Mater High Temp 33(4–5):549–559. https://doi.org/10.1080/09603409.2016.1183068
2. Bewlay BP, Weimer M, Kelly T, Suzuki A (2013) The science, technology, and implementation of TiAl alloys in commercial aircraft engines. Mater Res Soc Symp Proc 1516:49–58. https://doi.org/10.1557/opl.2013.44
3. Eylon D, Keller MM, Jones PE (1998) Development of permanent-mold cast TiAl automotive valves. Intermetallics 6(7–8):703–708. https://doi.org/10.1016/s0966-9795(98)00036-3
4. Loretto MH, Godfrey AB, Hu D, Blenkinsop PA, Jones IP, Cheng TT (1998) The influence of composition and processing on the structure and properties of TiAl-based alloys. Intermetallics 6(7–8):663–666. https://doi.org/10.1016/s0966-9795(98)00035-1
5. Voice W (1999) The future use of gamma titanium aluminides by Rolls-Royce. Aircraft Engineering and Aerospace Technology 71(4):337–340(4). https://doi.org/10.1108/00022669910371031
6. Schuster JC, Palm M (2006) Reassessment of the binary aluminum-titanium phase diagram. J Phase Equilib Diffus 27(3):255–277. https://doi.org/10.1361/154770306X109809
7. Kim Y-W (1994) Ordered intermetallic alloys, part III: gamma titanium aluminides. Jom 46(7):30–39. https://doi.org/10.1007/BF03220745
8. Paul JDH, Appel F, Wagner R (1998) The compression behaviour of niobium y-titanium aluminides. Strain 46(4):1075–1085
9. Huang SC (1993) Alloying considerations in gamma-based alloys. In: International symposium on structural intermetallics, pp 299–307
10. Bryant MJ, Christodoulou L,Maisano JR (1990) Effect of TiB2 additions on the colony size of near gamma titanium aluminides. Scr Met Mater 24(1):33–38. https://doi.org/10.1016/0956-716X(90)90562-U
11. Arenas MF, Acoff VL (2004) An investigation of the cracking susceptibility of gamma titanium aluminide welds produced by gas tungsten arc welding. High Temp Mater Process 23(1):25–34. https://doi.org/10.1515/HTMP.2004.23.1.25
12. Chaturvedi M, Richards N, Xu Q (1997) Electron beam welding of a Ti–45Al–2Nb–2Mn + 0.8 vol.% TiB2 XD alloy. Mater Sci Eng A 239–240:605–612. https://doi.org/10.1016/s0921-5093(97)00637-0
13. Jicai F, Huiqiang W, Jingshan H, Bingang Z (2005) Microstructure evolution of electron beam welded Ti3Al-Nb joint. Mater Charact 54(2):99–105. https://doi.org/10.1016/j.matchar.2004.11.006
14. Reisgen A, Olschok U, Backhaus S (2010) Electron beam welding of titanium aluminides – Influence of the welding parameters on the weld seam and microstructure. Mater Werkst 41(11):897–907
15. Chen G, Zhang B, Liu W, Feng J (2011) Crack formation and control upon the electron beam welding of TiAl-based alloys. Intermetallics 19(12):1857–1863. https://doi.org/10.1016/j.intermet.2011.07.017
16. Kuwahara M, Yamaguchi G, Nanri S, Ootani K (2000) CO2 laser welding of titanium aluminide intermetallic compound. In: Proc. SPIE 3888, High-Power Lasers in Manufacturing
17. Cam G, Kocak M (1999) Diffusion bonding of investment cast γ-TiAl. J Mater Sci 34(14):3345–3354. https://doi.org/10.1023/A:1004624930352
18. Çam G, Ipekoğlu G, Bohm KH, Koçak M (2006) Investigation into the microstructure and mechanical properties of diffusion bonded TiAl alloys. J Mater Sci 41(16):5273–5282. https://doi.org/10.1007/s10853-006-0292-4
19. Wang XR, Yang YQ, Luo X, Zhang W, Zhao GM, Huang B (2013) An investigation of Ti-43Al-9 V/Ti-6Al-4 V interface by diffusion bonding. Intermetallics 36:127–132. https://doi.org/10.1016/j.intermet.2012.12.018
20. Simões S, Viana F, Koak M, Ramos AS, Vieira MT, Vieira MF (2011) Diffusion bonding of TiAl using reactive Ni/Al nanolayers and Ti and Ni foils. Mater Chem Phys 128(1–2):202–207. https://doi.org/10.1016/j.matchemphys.2011.02.059
21. Simões S et al (2010) Diffusion bonding of TiAl using Ni/Al multilayers. J Mater Sci 45(16):4351–4357. https://doi.org/10.1007/s10853-010-4303-0
22. Mirski Z, Rózański M (2013) Diffusion brazing of titanium aluminide alloy based on TiAl (γ). Arch Civ Mech Eng 13(4):415–421. https://doi.org/10.1016/j.acme.2013.04.007
23. Ustinov AI, Falchenko YV, Ishchenko AY, Kharchenko GK, Melnichenko TV, Muraveynik AN (2008) Diffusion welding of γ-TiAl based alloys through nano-layered foil of Ti/Al system. Intermetallics 16(8):1043–1045. https://doi.org/10.1016/j.intermet.2008.05.002
24. He P, Feng JC, Xu W (2005) Interfacial microstructure of induction brazed joints of TiAl-based intermetallics to steel 35CrMo with AgCuNiLi filler. Mater Sci Eng A 408(1–2):195–201. https://doi.org/10.1016/j.msea.2005.08.009
25. He P, Feng JC, Xu W (2006) Mechanical property of induction brazing TiAl-based intermetallics to steel 35CrMo using AgCuTi filler metal. Mater Sci Eng A 418(1–2):45–52. https://doi.org/10.1016/j.msea.2005.11.005
26. Lee WB, Kim YJ, Jung SB (2004) Effects of copper insert layer on the properties of friction welded joints between TiAl and AISI 4140 structural steel. Intermetallics 12(6):671–678. https://doi.org/10.1016/j.intermet.2004.02.004
27. Davies P, Johal A, Davies H, Marchisio S (2019) Powder interlayer bonding of titanium alloys: Ti-6Al-2Sn-4Zr-6Mo and Ti-6Al-4 V. J AdvManuf Technol 103:441–452. (2019). https://doi.org/10.1007/s00170-019-03445-3
28. Forsdike J (2009) Novel joining and repair of aerospace. Swansea University, Singleton Park
29. Brady GS, Clauser HH, Vaccari JA (2002) Materials Handbook, 15th edn. McGraw-Hill, Toronto
30. Davies P, Davies H, Marchisio S (2019) The bonding of additive manufactured Ti-6Al-4 V via the powder interlayer bonding (PIB) process. In: The 14th World Conference on Titanium
31. Stanners O, John S, Davies H, Watkins I, Marchisio S (2019) The effect of processing variables on powder interlayer bonding in nickel-based superalloys. Materials: Advances in Structural Metallic Systems for Gas Turbines. https://doi.org/10.3390/ma13030601
32. Watkins IT, Davies HM, Stanners OG,Marchisio S (2019) Powder interlayer bonding of geometrically complex Ti-6Al-4 V parts. Int J Adv Manuf Technol 106:3629–3639. https://doi.org/10.1007/s00170-019-04685-z
33. Djohari H, Martínez-Herrera JI, Derby JJ (2009) Transport mechanisms and densification during sintering: I. Viscous flow versus vacancy diffusion. Chem Eng Sci 64(17):3799–3809. https://doi.org/10.1016/j.ces.2009.05.018